Technology demonstration of starshade manufacturing for NASA's Exoplanet Mission Program

N. J. Kasdin[a], D. Lisman[b], S. Shaklan[b], M. Thomson[b], E. Cady[b], S. Martin[b], L. Marchen[b], R. J. Vanderbei[a], B. Macintosh[c], R. E. Rudd[c], D. Savransky[c], J. Mikula[d], D. Lynch[d]

[a]Princeton University, Princeton, NJ, 08544 USA
[b]Jet Propulsion Laboratory, California Institute of Technology, Pasadena, CA, 91109 USA
[c]Lawrence Livermore National Laboratory, Livermore, CA, 94551 USA
[d] NASA Ames Research Center, Moffett Field, CA, 94035 USA

ABSTRACT

It is likely that the coming decade will see the development of a large visible light telescope with enabling technology for imaging exosolar Earthlike planets in the habitable zone of nearby stars. One such technology utilizes an external occulter, a satellite flying far from the telescope and employing a large screen, or starshade, to suppress the incoming starlight sufficiently for detecting and characterizing exoplanets. This trades the added complexity of building the precisely shaped starshade and flying it in formation against simplifications in the telescope since extremely precise wavefront control is no longer necessary. In this paper we present the results of our project to design, manufacture, and measure a prototype occulter petal as part of NASA's first Technology Development for Exoplanet Missions program. We describe the mechanical design of the starshade and petal, the precision manufacturing tolerances, and the metrology approach. We demonstrate that the prototype petal meets the requirements and is consistent with a full-size occulter achieving better than 10^{-10} contrast.

Keywords: External occulters, occulters, starshades, exoplanets, high-contrast imaging, TDEM

1. INTRODUCTION

This paper describes the final results of our ROSES Technology Development for Exoplanet Missions (TDEM) program. Our goal was to advance the readiness of one of the most challenging technologies associated with occulter-based planet finding and characterization—manufacturing a large starshade to the needed accuracy. To that end we, for the first time, built a full-scale occulter petal, using flight-like processes and materials, and to near-flight tolerances as they are presently understood. We then performed metrology to confirm that the critical shape requirements had been met and our contrast goal achieved.

We show in this paper that a precision starshade petal can be manufactured to meet the shape requirements corresponding to a contrast consistent with our error allocation. To accomplish this, we simulated a full starshade populated by petals identical to the manufactured one. We then used our optical modeling tools to propagate an incident field to the image plane of the telescope and predicted the resulting contrast. We repeated a sufficient number of times to give us statistical confidence in our predicted contrast. We chose a relaxed requirement from flight of 10^{-9} total contrast (3×10^{-10} allocated to manufacturing) as our success criteria as this is the first time any petal will have been built to flight tolerances, making a relaxed requirement appropriate. Our established milestone for this TDEM study was thus stated as follows:

> On a single full-scale petal made of flight-like materials, measure the width of the optical edges at a sufficient number of locations and with sufficient accuracy to show that, using modeling, the mean contrast in the image plane from a uniform field propagated past an occulter with petals of the measured shape in an annulus of width equal to the full-width half-max of the telescope

Send correspondence to jkasdin@princeton.edu

Space Telescopes and Instrumentation 2012: Optical, Infrared, and Millimeter Wave, edited by Mark C. Clampin, Giovanni G. Fazio, Howard A. MacEwen, Jacobus M. Oschmann, Jr., Proc. of SPIE Vol. 8442, 84420A
 · doi: 10.1117/12.926790

point spread function at the smallest inner working angle is 3×10^{-10} or better, the allocated contrast to static errors. We repeat the measurements and analysis a sufficient number of times to give 95% confidence that the predicted contrast is correct.

Our accomplishments against this milestone were the following:

1. We successfully manufactured, assembled, and measured a full-size occulter petal out of flight-like materials using close to flight-like processes. Metrology results show the shape meets the requirements in the error budget for a flight-quality occulter.
2. We did better than the milestone for contrast from a modeled occulter made of petals with the same measured shape. The expected value of the contrast from an occulter made up of 30 petals identical to the as-built petal is better than 2.15×10^{-10} at the smallest inner working angle and at all wavelengths of interest. Using a statistical analysis of the measurement error, we have 95% confidence that the contrast is better than 2.16×10^{-10} for the worst case wavelength, 30% better than our milestone value.
3. We showed that the more realistic case of an occulter made up of 30 petals with random manufacturing errors consistent with those seen in our measured as-built petal results in an expected contrast of 2.12×10^{-11} with a 95% confidence value of 4×10^{-11} at the worst case wavelength.

In addition, we measured microcracking in composite coupon samples undergoing strains similar to those experienced in the stowed occulter petal. No large cracks were found ($>$ 100 microns) in either critical or non-critical structural elements for strains up to the maximum design level of 0.5% strain. Analysis is ongoing to quantify nanocracking at lower strain.

There were several secondary goals that we did not accomplish. Foremost was work on the precision, tapered optical edge. A precision optical edge serves to both determine the final optical width of the petal as well as to ensure solar scattering is minimized. While the final occulter as-built did have a precise edge that met the shape requirements, it did not have the sharp taper needed to minimize scatter. We had hoped, on a best effort basis, to develop manufacturing concepts for producing sharp edges and to test the scatter from edge coupons. Unfortunately, the design and development work proved beyond the scope of the resources available and would have delayed or distracted from the primary objective. We also had concerns that available metrology would be ineffective with the sharp edge. (In a future development program we would expect that a more sophisticated laser metrology system would be used.) We therefore opted for a straight, vertical edge in the as-built petal. We had also hoped that resources would allow a stow and deploy test of the as-built petal with additional post-deployment metrology. Unfortunately, we were not able to conduct such a test with the funding available.

Nevertheless, the program was a significant success and demonstrated the viability of building full scale occulter petals that meet the stringent shape requirements for the very high contrast needed in a flight system. The remainder of this paper describes the approach we took and the results we obtained in more detail. Section 2 provides an overview of the occulter design we used for testing, Section 3 describes how we allocate shape errors in an overall error budget, Section 4 describes the mechanical design concept, Section 5 summarizes the materials and manufacturing process for the petal, Section 6 describes the process for measuring the final petal shape, and Section 7 describes how we converted those measurements into estimates of contrast with confidence intervals.

2. DESIGN OVERVIEW

Our approach to designing occulters uses optimization tools to determine the apodization that results in the smallest and closest possible occulter while still achieving the starlight suppression requirement over a desired wide spectral band.[1] This emphasis on minimizing size makes it easier to manufacture and handle, reduces the size of the launch vehicle and fairing, and increases the potential science yield. Hence, the requirements

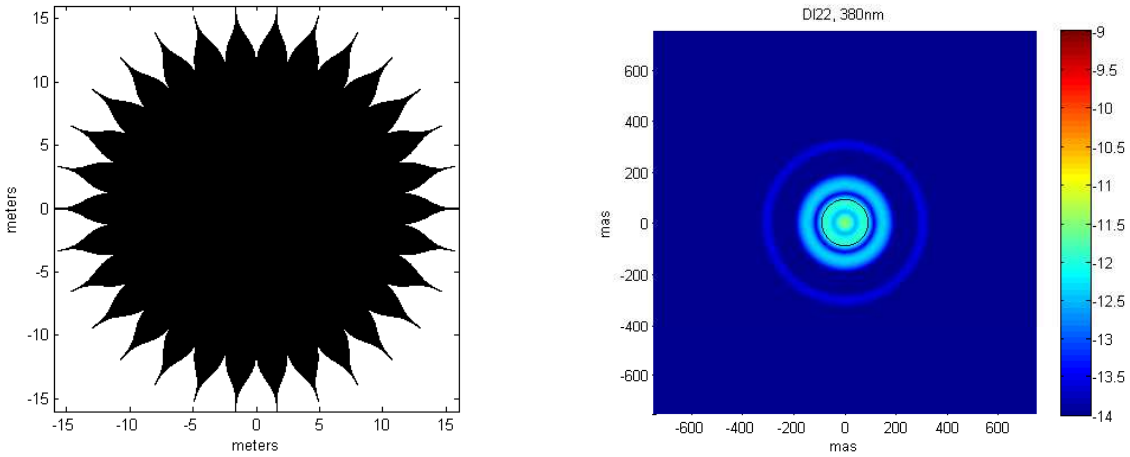

Figure 1. *(Left)* The DI22 occulter designed for 1.5 m telescope being used for this TDEM study. It is 32 m in diameter with 30 petals, each 6 m long and 2.34 m wide at the widest point. *(Right)* The corresponding PSF at 380 nm in the telescope image plane. Telescope is on-axis with a 30% obstruction. Circle indicates inner working angle.

we describe here are the tightest possible, specifying the allocated contrast at the smallest inner working angle of the smallest possible occulter. (Larger occulters result in relaxed tolerances.)

There are several mission concepts at various scales for which we have designed and analyzed occulters. For this study, we have modified our O_3 design* to incorporate a 1.5 m telescope, thus making the image plane contrast slightly less sensitive to occulter errors and easier to fit in the facility. The resulting two-distance occulter, dubbed DI22 and shown in Figure 1, is 32 m in diameter with 6 m long petals and a slightly larger IWA than a flagship size mission, 90 mas rather than 75 mas. It operates over the same pair of wavelength bands as O_3: 250-550 nm at a distance of 36670 km and 500-1100 nm at a distance of 18335 km. We have also designed the occulter for 30 petals to lower the cost and simplify the manufacturing for this first test. With 30 petals, each petal has the desired length and a width at the widest point of 2.34 m, which makes it more manageable for our existing facilities. This comes at the expense of smaller gaps between petals and narrower tips (1 mm). An eventual flight design would most likely have fewer, but wider, petals (as few as 16) with correspondingly larger gaps and tips (up to 2 mm).

3. ERROR BUDGET

Any realistic engineering design of the occulter can only meet the desired shape to within certain realizable tolerances. Additionally, the operation of the occulter through varying thermal environments and dynamic loading will inevitably cause variations in the shape. Shaklan et al.[4] describe in detail the modeling approach used to develop engineering requirements and determine the sensitivity of the design to errors in manufacture and variations in flight. An optical modeling tool has been developed, described there, that finds the image plane response of the telescope past an occulter with various errors. It is important to base all error budgeting on image plane simulations as different errors may diffract light to different locations in the image plane and thus have more or less impact on the ability to extract a close in planet.

After completing the petal, we updated the error budget to better represent errors encountered in the building and measuring of the TDEM petal. In particular, before building the petal we had modeled petal shape perturbations as ideal edge segment displacements and tilts combined with sine waves running the length of the petal, in addition to global size and shape errors.[4] After building the petal using high-precision

*O_3, or the Occulting Ozone Observatory, was a mission concept for a 1.1 m telescope and 30 m tip-to-tip occulter with 24 7.5 m long petals. It had the capability to detect planets down to Earth size, perform photometric characterization, detect the present of ozone, and do general astrophysics.[2,3]

Perturbation	Amplitude (1σ)	Contrast	Wavelength (nm)
Segment δx	20 μm	5.3×10^{-13}	550
Segment δy	20 μm	6.6×10^{-12}	550
Segment In Plane Tilt	20 μrad	1.6×10^{-12}	550
Segment Placement Total		8.8×10^{-12}	550
1 cycle/segment	15 μm	1×10^{-11}	300
2 cycle/segment	15 μm	7.7×10^{-13}	300
3 cycle/segment	10 μm	2×10^{-13}	250
4 cycle/segment	10 μm	8.1×10^{-14}	250
5 cycle/segment	10 μm	4.4×10^{-14}	250
6 cycle/segment	10μm	2.8×10^{-14}	250
Segment Shape Total		1.1×10^{-11}	250
Proportional Width	5×10^{-6}	7×10^{-14}	550
Tip Clip	1 mm	1.15×10^{-13}	250
Quadratic Out-of-Plane Bend	5 mm	6.3×10^{-15}	550
Quadratic in-Plane Bend	250 μm	9.5×10^{-17}	550
Non-Segment Manufacture		1.3×10^{-13}	550
Random Error Total		1.5×10^{-11}	550

Table 1. Worst-case allocated errors to each of the top 13 perturbations to meet the total allocated contrast due to random petal errors of 1.5×10^{-11}. All errors are 1σ based on an assumed Gaussian distribution among all segments. Global errors contribute less than 30% of the total contrast due to the nominal contrast plus all manufacturing errors.

(5μm) metrology to define fiducials along the edge, we found that it was no longer necessary to carry sine wave errors along the full petal length; rather, we replaced them with sine wave shape errors on each of the segments. We also found that, contrary to our initial expectations, global petal errors are unlikely to play a significant role in the error budget. We initially thought that our prediction of contrast would be limited by our metrology, suggesting that global systematic errors could be a problem. However, our experience showed that the residual contrast is dominated by construction and assembly errors, which are expected to be random. Thus, our updated budget mainly considers random errors from petal-to-petal, not global ones.

The error budgeting tool is an Excel spreadsheet that reads sensitivity files generated from propagation models. We compute the image plane mean and r.m.s. contrast for a given amplitude of each perturbation (e.g., a 100 μm sine wave of 3 cycles per segment on segment 1) over a 1 λ/D annulus centered at the inner working angle and evaluate at 7 wavelengths spanning the starshade bandpass (0.25–0.55 μm for the TDEM starshade) assuming a Gaussian distribution of error. The contribution of a given perturbation to the residual contrast scales as the square of the perturbation amplitude. We treat all perturbations as independent and combine the coherent background scatter, local (speckle-like) scatter, and radially symmetric scatter following the approach described in Shaklan et al (2010).[5]

In addition to the segment placement and shape errors, we also consider proportional width and in-plane and out-of-plane quadratic bends on the petals. The proportional width error was originally conceived to account for long-range metrology errors that could be significant over the width and length of the petal, and smaller closer to the tip of the petal. We have found that the combination of the high-precision metrology used to define the petal mechanical structure with small-distance metrology used to place the segments prevented the buildup of significant proportional width errors. As described in Section 6 the runout errors in the CMM used to define the optical edge were less than $\sim 5\mu$m. The metrology used to determine placement of the optical edges was accurate to $\sim 10\mu$m over the short range used, but errors were random from segment to segment so no large-scale metrology error could accumulate. Thus the proportional width error is limited to no more than about 10μm which our analysis shows contributes less than 1×10^{-13} to contrast. (For the case of proportional width error, the global allocation is larger than the random one.)

Our original goal was to create a petal whose manufacturing errors led to less than 3×10^{-10} contrast. This

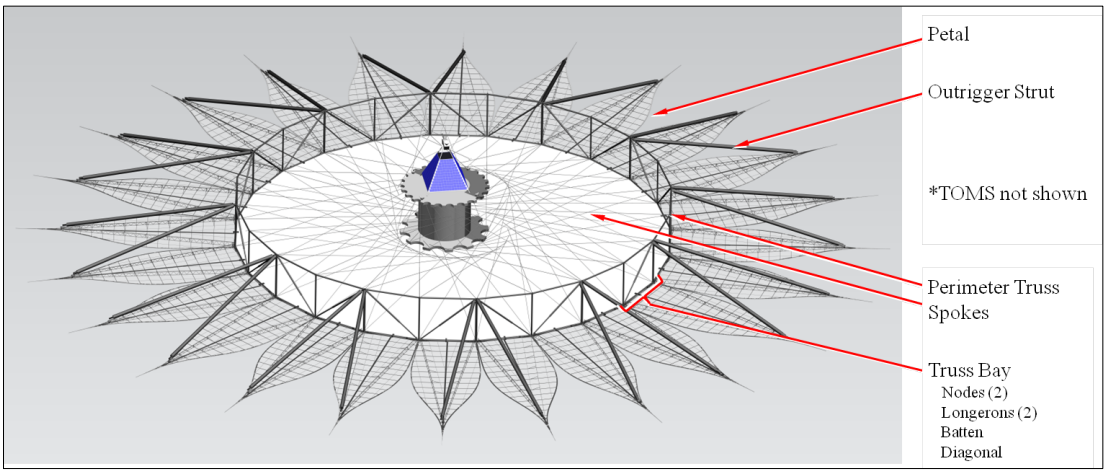

Figure 2. Deployed starshade.

value was selected to be a fraction of a conservative and relaxed overall starshade performance requirement of 1×10^{-9} contrast allocated to manufacturing errors. We also specified the milestone based on the most conservative assumption of identical (global) errors on each of the 30 petals. Even with this conservatism our resulting petal achieved a 30% better contrast than the milestone when assuming all errors are global.

As we explained at the beginning of the section, however, our experience in manufacturing and measuring the petal shows that we are dominated by random manufacturing errors rather than global systematics. Our results analyzing the measured shape of the occulter also show that our as-built petal shape errors, when considered as random errors on each petal, correspond to an overall contrast closer to a flight starshade designed for 10^{-10} rather than the relaxed 10^{-9} of the milestone (see Section 7.2). We thus have updated our error budget to correspond to this lower flight-like occulter contrast with an allocated contrast to random petal manufacturing errors of 1.5×10^{-11}. Table 1 shows one allocation of errors to the dominant terms that meets this allocation at the worst case wavelengths. Because the contrast is dominated by the random petal-to-petal errors (the global errors contribute roughly 30% of the total residual contrast at the worst case wavelength) we only include the allocation to random errors here for brevity. Including an allocation for the global errors (dominated by the low frequency, 1 cycle/segment error on each segment) and the nominal contrast (roughly 7×10^{-13}) results in a total allocated contrast for manufacturing of 2×10^{-11} .

4. MECHANICAL DESIGN SUMMARY

A schematic of the deployed star shade is shown in Figure 2. The petals are arrayed around the circumference of a deployable perimeter truss (derived from the AstroMesh reflector antenna developed by Northrop Grumman Aerospace Systems (NGAS)). The petals employ a highly mass efficient lattice structure comprised of pultruded graphite fiber reinforced plastic (GFRP) rods that have finely tuned CTEs to limit thermal deformations. The lattice structure is configured and optimized to provide stiffness and stability as required to meet petal stability requirements. When stowed, the starshade petals are wrapped around a fixed, lightweight central hub structure. The hub is sized to provide sufficient annular radius between its OD and the fairing ID to contain the stowed starshade truss and petals while maximizing hub diameter to reduce petal strain. The TDEM petal is designed to work with a 3 m hub. The petals wrap approximately 2/3 of the way around the hub circumferentially and overlap about 2/3 of the total stowed truss height vertically.

Figure 3 details the petal structural design, as viewed from the telescope (anti-sun) side, with the Thermo-Optical Micrometeorite Shield (TOMS) blanket removed. The primary petal structure is a lattice of battens and longerons that intersect a longitudinal spine and a pair of structural edges on each side. These elements are optimized to place and precisely maintain the optical edge with the required profile tolerance regardless

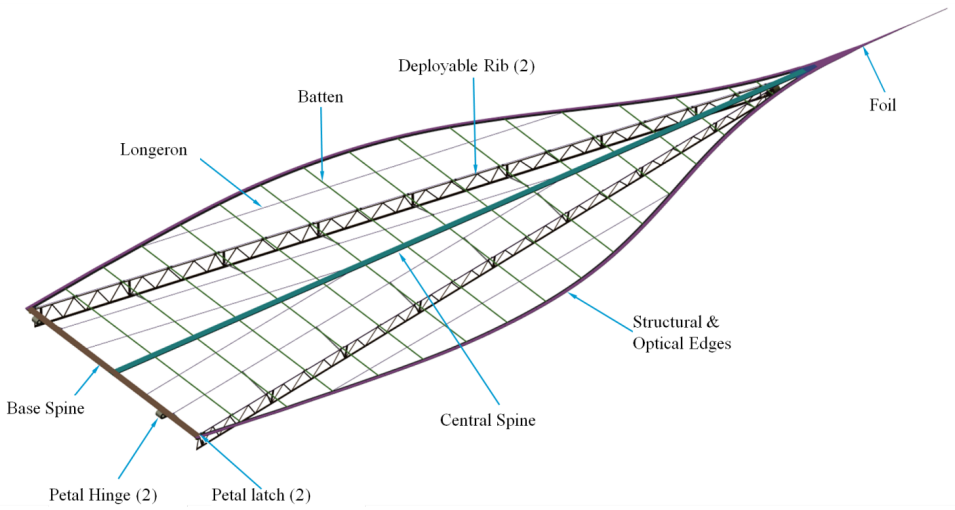

Figure 3. Petal mechanical design.

of thermal extremes or structural loads from the relatively thermally unstable TOMS. The lattice is highly mass efficient yet very stiff in-plane. Secondary petal structure includes a pair of deployable ribs in an "A" frame configuration that stiffen and maintain overall deployed petal flatness. The deployable ribs fold outward and flat against the petal when stowed then pop up into place when the petal is unfurling. The ribs are deployed by extension springs that are inside hollow soda-straw size GFRP struts that lock the ribs in place at a near-perpendicular angle to the petal when deployed. The ends of the deployable ribs coincide with truss-to-petal interface nodes on the base spine and with the outboard end of the outrigger at the apex of the "A" to complete the tripod-like geometry of the petal and outrigger support structure on the edge of the perimeter truss. Because we had hoped to find the resources to perform a stow-and-deploy test of the petal we manufactured ribs for the TDEM petal. These were not installed, however, for the metrology tests and resources were not available to perform the deployment.

The battens define and maintain the precise petal edge-to-edge width. They are made from a pultruded GFRP base material with a near-zero room-temperature axial CTE. The battens are continuous across the width of the petal so that joints will not affect their axial stability. Longerons provide the petal with in-plane shear stiffness for maintenance of the overall shape, though this is limited by the long aspect ratio of the petal. They are expected to be made from the same pultruded GFRP as the battens (though slightly different materials were used for the TDEM), have a circular cross section and are also continuous along their length. The longest pair of longerons also act as hinge pins for the deployable ribs. Like the battens, the number and placement of longerons is somewhat arbitrary. The longitudinal and base spines provide additional stiffness and are constructed of a foam core sandwiched between thin graphite face sheets. The base spine closes out the petal root structure and carries the perimeter truss interfaces: two hinge points for the unfurling portion of deployment and two precise latches that position the deployed petal in-plane.

All petal structures are designed so that no component is subjected to more than 0.5% strain (5000 μstrain) when stowed around the 3m diameter hub, ensuring that permanent plastic deformation or material creep that would degrade the deployed shape or figure of the starshade will not occur. The maximum strain is only approached in the longitudinal spine and our current design shows a maximum of only 0.2%, a 150% margin. The spine also has little or no role in the definition of the deployed petal edge profile. Its primary function is to accommodate launch restraints and deployment hardware and as a ground-handling interface. The battens are perpendicular to the direction of stowed petal strain and thus will not experience permanent set prior to launch.

The 25mm wide and 0.4mm thick graphite composite optical edges are manufactured separately from

the petal in the longest lengths practical for maintaining the required figure profile; between 0.8m and 1.3m long. The segments are aligned using a FARO coordinate measuring machine (CMM) and then secured with precision clamps for a room temperature cure bonding process. The petal tip is bolted into a transition plate that connects the central spine and edges together.

5. PETAL MANUFACTURING

In this section we describe the manufacture and assembly process of the TDEM petal.

5.1 Material Selection

Most petal components are constructed of carbon composite materials for the sake of mass efficiency and stability. Exceptions include the spine foam cores, assembly parts and hinges. Battens are commercially available hollow carbon pultruded rods made of Toho IMS60 E13 fibers and premium grade bisphenol epoxy vinyl ester resin and of 0.25in square section. The longerons are also solid pultruded rods but are made of a similar Toray T-700 S fibers with the same premium grade bisphenol epoxy vinyl ester resin. They are .125in round cross section. The tested CTE over the temperature range of interest for both materials is better than $-0.2 \times 10^{-6}/^{\circ}\mathrm{C}$, which is adequate for this application, but can be reduced further by optimizing the fiber verse resin types and ratios. The pultrusion process yields unidirectional fibers with a precisely controlled resin volume ratio, for uniform and controllable CTE performance.

Structural edges are machined from a high-modulus quasi-isotropic GFRP carbon composite laminate using Toray M55J fibers and Patz Materials and Technologies PMT-F6 cyanate-ester resin in a [60/-60/-60/60/0/0/60/-60/-60/60/0/symmetric] laminate with 0.0045in thick plys. They are thus approximately 0.10in thick and 1.2in wide. The deployable ribs are machined from this same laminate although they were not installed in the TDEM petal during the current phase of the project.

Optical edges are made from a GFRP laminate similar to the structural edges, but have 0.003in thick plys in a [60/-60/0/0/-60/60] laminate resulting in a much thinner (0.018in thick) material. The fiber orientation in the manufactured optical edges is critical to avoid the possibility of having any fiber direction being close to parallel (or tangent) to the overall in-plane profile of the optical edge profile, i.e., we cut "across the grain." This makes it possible for the shape of the optical edge to be maintained to the highest possible degree both during manufacture and upon handling and long-term use. Strands of parallel/tangent fibers on the 25-50 micron radius cross-sectional profile would otherwise be easily shed due to minute stress risers between fibers and resin. On average, the fibers are oriented perpendicular to and ± 30 degrees from the nominal cut direction, noting that the edges are curved in shape.

The spine face sheet ply thickness and laminate schedules are identical to the optical edges. The fiber orientation in the manufactured spine face sheet parts, however, is rotated 90 degrees to allow the laminate zero-degree fibers to be parallel to the parts, which is desirable in this case.

5.2 Manufacturing Process

The battens and longerons were purchased from Diversified Composites in Erlanger Kentucky in special runs to produce very long, straight pieces. They were cut to length and then the battens were machined using a CNC router for the slots that the structural edges and holes that the longerons are bonded into. The other parts were machined from large sheets of GFRP. JPL provided the M-55J fibers from excess flight materials and Patz Materials and Technologies prepared two different resin impregnated tapes (pre-preg). A second company performed the layup and curing (Applied Aerospace Composites, AASC) and a third company performed the machining (Roncelli Plastics).

Experiments were performed to determine if a beveled edge with the desired radius of curvature could be machined with a router. This effort was not successful and abandoned due to cost and schedule constraints. A decision was made to proceed with optical edges with square cuts and defer development of beveled edges.[†]

[†]A development program for beveled edges is now underway at Vanguard Space Technologies, Inc under their NASA SBIR 2011.

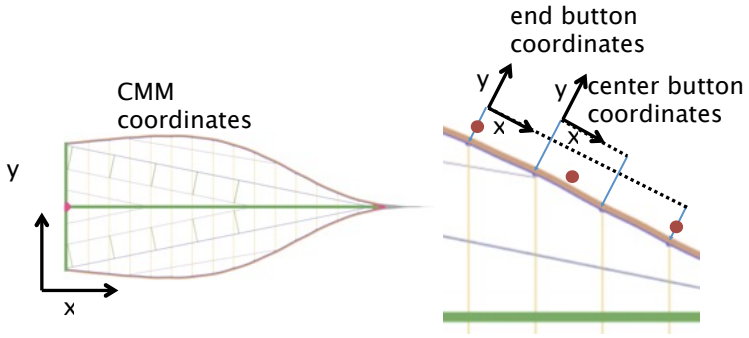

Figure 4. A schematic of the global and local coordinate systems used for optical edge placement.

Additional experiments were performed to determine optimal cutters, cutter speed, feed-rates, feed direction and hold-down methods. The selected hold-down method was to sandwich the GFRP sheet between 2 thick sheets of phenolic plastic bolted together and bolted to the router table. The parts were lightly sanded to remove burs at the top and bottom faces but care was taken not to touch the middle layers, which define the edge profile.

The petal structure was assembled starting with the base spine and then positioning the battens and bonding them to one face of the central spine. Foam core was then added to the central spine in between the battens and then the second face sheet was bonded to the central spine. The structural edges were installed next, followed by the longerons. The optical edges extend over the structural edges by 0.25 in.

5.3 Optical Edge Installation

The optical edge on each side is divided into 5 segments about 40in long (an additional piece would form the tip) for ease of handling and installation. A FARO Advantage Platinum, 8ft reach portable measurement arm was used to position the optical edges onto the mechanical edge. The FARO has a reach of approximately 96in side-to-side and therefore is capable of measuring across the entire width of the petal. However, the FARO has a limited accuracy of about 30 micron per meter, resulting in large errors at the extremes of the reach. Since it was desired to set the edges to 10 micron accuracy, a system of calibrated buttons on the optical and structural edge was developed to limit the use of the FARO to short range where an accuracy of approximately 8 microns could be achieved. Each piece of the optical edge thus has five buttons installed into holes evenly spaced along its length starting approximately 1 in from either end. The buttons consist of a conical hole drilled into a flanged part that is glued into the edge section to form a set of fiducial positions. A second set of buttons is set into the mechanical edge, two on either side of each batten. With the distance between battens being approximately 10in, the optical edges are set with ends adjacent to a batten. This results in four sets of buttons on the mechanical edge per optical edge section, and five sets on the optical edge itself. Buttons placed near to the ends of the optical edge segment and near to the batten ends would be only 1 in or so apart, enabling the FARO's best accuracy to be achieved at these locations.

All structural button positions are defined relative to a global coordinate system with origin at the center of the full occulter, and the x-axis passing through the center of the petal. (Selecting this coordinate system allowed the edge shape, as designed by optimization, to be aligned with respect to the buttons without translation or rotation.) In addition, each pair of buttons on the mechanical edge is used to define a local coordinate system with origin at one of the buttons, x-axis toward the next pair of buttons and y-axis perpendicular. The FARO is used independently in each local coordinate system for optical edge placement to ensure that it is only used over short ranges. The global and local coordinate system is schematically shown in Figure 4. To properly calibrate the short range use of the FARO, independent measurements of each button location in the global coordinates was made at Allied mechanical prior to the assembly in August 2011 using their DEA model Delta SP 512518 CMM machine. The resulting median measurements were used as the "truth standard" for the location of each structure button. All subsequent placement was

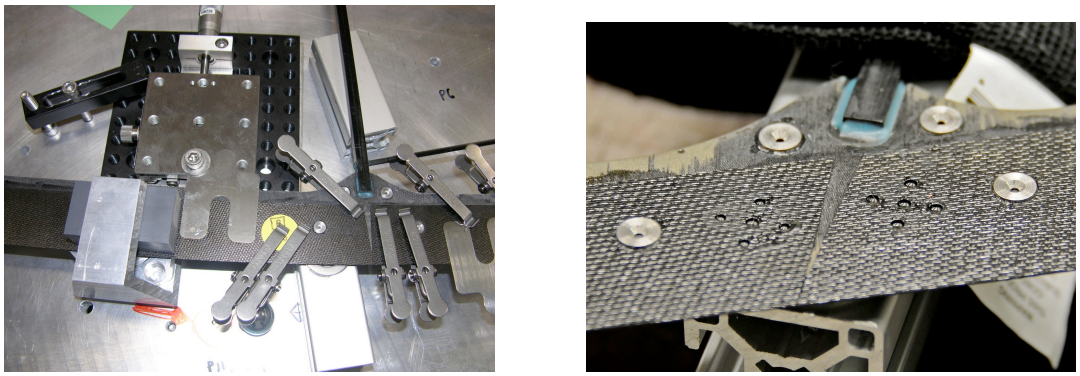

(a) (b)

Figure 5. *(Left)* End of edge section showing translation stage and shim attachment used to adjust edge. Also shown are the metal clips and left, the aluminum and grey plastic spacer are part of the pneumatic clamp. *(Right)* Detail of the junction of two edge pieces showing the two batten-end buttons and the two edge piece end buttons. The pattern of five holes is the injection/relief holes for the epoxy bonds.

done with respect to these button locations. Repeatability of the measurements was within the expected 5μm accuracy of the Allied machine.

For edge installation, the petal was secured on a batten in one place near the FARO's base (bolted to the table) and in another near to the edge. This ensured that the petal remained fixed relative to the FARO arm but would be free to slide on the table so that potential thermally-induced distortions would be minimized. Having secured the FARO and the petal, a baseline was set up for the FARO, normally consisting of the two batten-end buttons which would be nearest to the optical edge ends, and a third point, normally on the base spine, to define the measurement plane. At the ends of the petal where the distribution of buttons was different, the nearest available structural buttons were used.

Next the optical edge was placed onto the structure and manually positioned to within 1 mm of its eventual location. A rule was placed along the line between the endmost structural buttons of the section and three linear translation stages positioned so that they would translate in a direction perpendicular to the line. After securing a stage to the table, a thin shim was placed to cross between the stage and the optical edge. Two small spots of cyanoacrylate adhesive were used to secure the shim to the optical edge. A bolt and washer secured the other end of the shim to the translation stage as shown in Figure 5(a). This bolt and washer combination could be released and retightened to alleviate strain when the optical edge was repositioned.

Next, the FARO ball was placed into the optical edge's end button and the two-axis stage adjusted to bring the button to its correct coordinate. Then the edge was clamped at the button to the structural edge using min-spring clamps shown in Figure 5(a) (McMaster-Carr type 5015A2). These clamps are 17-7 PH stainless steel with an Inconel X-750 spring and have smooth clamping surfaces to prevent marring. Approximately 10 of the clips were fastened along the edge to ensure strain-free positioning and good contact with the structural edge. By an iterative process of clamping, unclamping and adjustment the two ends were brought to their correct coordinates while producing minimal strain in the edge. The longitudinal position of only the end button nearest the base spine was set; the other end was allowed to float in that direction, producing minimal longitudinal strain.

Once the two end buttons were positioned, pneumatic clamps were activated to firmly fix the ends. After rechecking the end button positions to ensure they had not moved, the intermediate clips were removed and the center button adjusted to bring its transverse position to the correct coordinate. Once a strain free position was achieved this center button was pneumatically clamped.

Finally, the edge was bonded to the structure in two stages. First, a line of cyanoacrylate adhesive was run along the inboard edge of the optical edge to adhere it to the structural part. This adhesive could

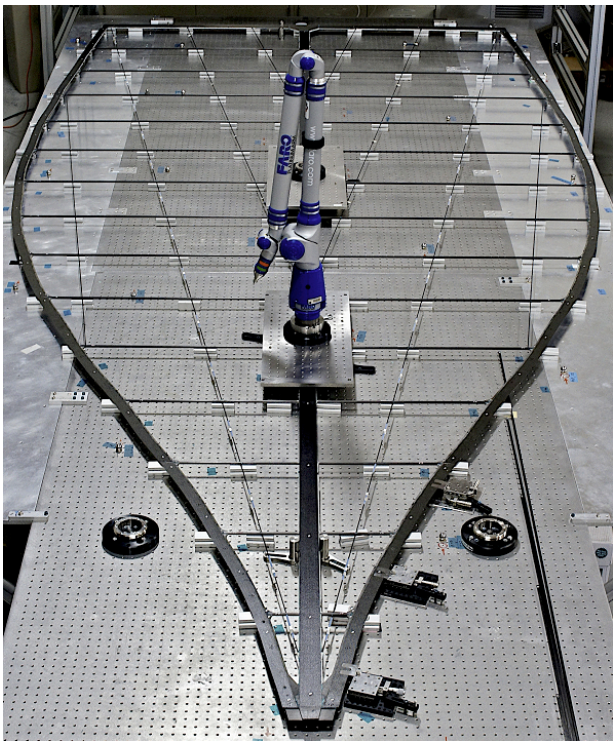

Figure 6. Assembled petal on the table at JPL, supported by small sections of aluminum extrusion extending onto the table extensions. The FARO arm is mounted on a bridge over the central spine. Translation stages are in position for adjustment of the right tip-most edge segment.

be softened using acetone and cut with a knife if removal was later required. Later, after all the edges were in place and the measurements showed satisfactory positioning, the edges were glued using Hysol 9320 epoxy adhesive injected into pits milled into the structural edge to form a permanent strong attachment. Figure 5(b) shows the finished junction of two edge pieces, the glue points and the button geometry. The fully assembled petal is shown in Figure 6.

6. MEASURING THE PETAL SHAPE

The final assembled petal shape was measured at Allied Mechanical over the 7th and 8th of February, 2012. These consisted of measurements of the entire optical edge made every centimeter, and of every button (excluding a few of the spine buttons). The petal was set up on two tables which were carefully adjusted to be coplanar, using longer pieces of extrusion as outriggers under the battens where the table width was less than the petal. To insure thermal stability during metrology the tables had been allowed to reach thermal equilibrium before setup. Four points were taken on each button flange, then the probe was dropped inside the button center to take four points inside the cone (shown in Figure 7). Then four more points were measured on the flange in a slightly smaller circle, and the probe dropped further inside the cone to take a second set inside the cone. The two sets of cone measurements would later be used to determine if the cone had been set into the edge at an angle.

The CMM machine measured the entire petal, buttons and edges, 5 times. Each time, a baseline was established from two base spine buttons and the longitudinal spines endmost button. Care was taken not to allow the petal to be touched by anything other than the CMM during the entire process. The measurement data was extracted between each set and compared with the expected differences in x and y between the structure and petal buttons from the previous set of measurements. Immediate analysis of this data showed

Figure 7. Cylindrical probe measuring inside the button at Allied. The edge of the cylindrical probe was also used to measure the edge location.

consistency between data sets and gave a preliminary indication of satisfactory results. Full analyses were made later at JPL and are described in the next section.

7. CALCULATING CONTRAST

In this section we summarize how we processed the Allied measurement data to arrive at an estimate of the expected contrast from an occulter made from the as-built petal. There are two sources of statistical variation that contribute to uncertainty, measurement error and manufacturing error. Ideally, a statistical confidence in our ability to meet requirements in manufacturing petals would be found by building and measuring many petals. This recognizes that the as-built petal is just a single member of a statistical ensemble of petals encompassing the expected variations in manufacturing. Building and measuring many petals would allow us to average both this manufacturing error and measurement error and come to reasonable estimates of both the mean contrast from an occulter built of similar petals as well as the standard deviation.

Clearly, however, this was not possible within the funding and schedule constraints of the project. Instead, we examined the more conservative success criteria that an occulter built from 30 petals identical to the as-built meets the contrast requirement. This is more conservative as global errors on the petals sum rather than average, producing a higher net contrast. The statistics of the computed contrast is then given only by the error in the edge measurements. We formed an independent estimate of the measurement error distribution based on calibration data supplied by Allied. The result, as we explain in Section 7.1 below, was an estimated distribution of contrast for an occulter made up of 30 petals with the best fit edge shape to our as-built and measured petal. This corresponds to the worst-case global error discussed in Section 3.

Fortunately, we can also say some things about the distribution underlying the manufacture of the petal. Because we built the optical edge in 10 separate segments, we were able to estimate the manufacturing statistics under reasonable assumptions of the independence of each segment. This allowed us to also calculate the contrast from an occulter populated with 30 different petals with random variations consistent with what we saw in the 10 optical edge segments we built. The result is an estimate of contrast that is more realistic and more consistent with our error budgeting process. We describe this in Section 7.2.

7.1 Milestone Contrast Calculation

To find the contrast from the petal as built, we used an average of the 5 Allied edge measurement data to simulate a complete starshade of 30 petals by rotating this shape about the origin by $\pi/15$ and replicating it, filling in the mm-scale gap at the truss boundary between the two with a circular arc; this was repeated for all 30 petals, and the shape was closed. As the tip was not built, the shape in this region was taken straight from the design. This closed curve was used as the input to an efficient line-integral-based propagator[6] which

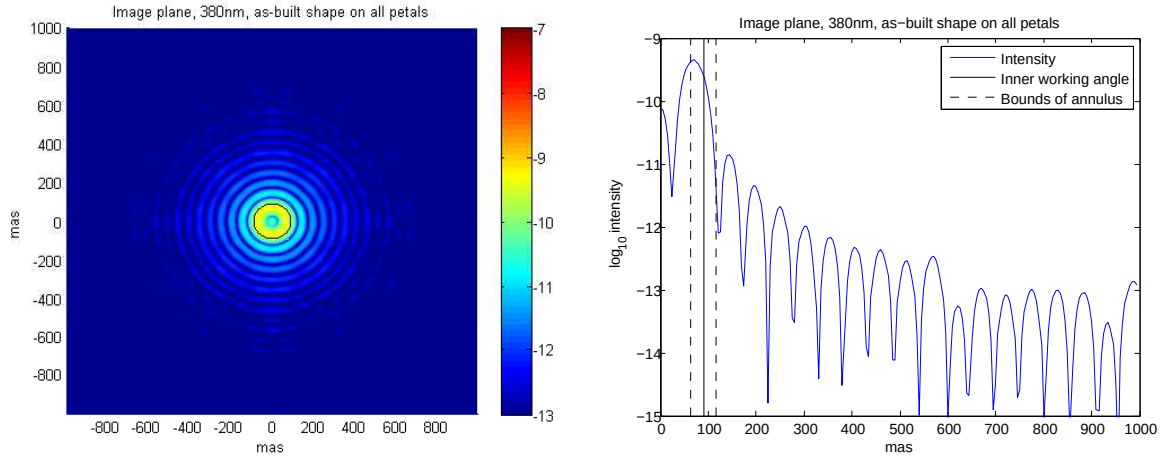

(a) Worst-Case PSF (b) PSF Cross Section

Figure 8. (*Left*) The image-plane intensity profile at 380nm for an occulter with 30 identical petals, plotted on a log scale. The inner working angle is shown with a solid circle. While the occulter is assumed to be spinning, this represents an instantaneous snapshot of the intensity. (*Right*) A cross section of the point-spread function showing the designed inner working angle and the boundaries of the annulus used for contrast calculation.

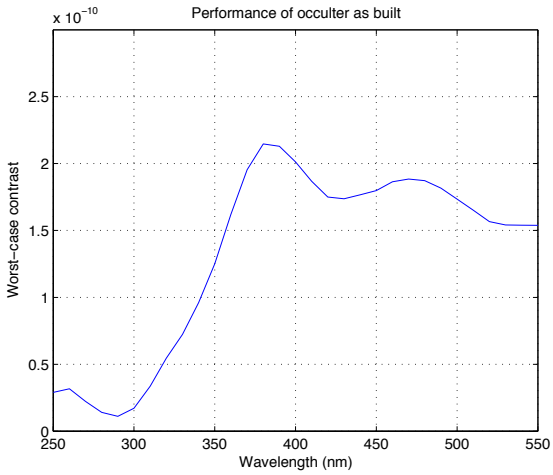

Figure 9. A plot of mean contrast in an annulus about the IWA for an occulter with 30 petals identical to the one built, plotted as a function of wavelength. The worst case is at 380nm, when the mean is 2.15×10^{-10}.

does not require analytic representation of errors to evaluate the field downstream. We then propagated the resulting shadow through a telescope—assumed to have an unobscured aperture—to the image plane and calculated a figure of merit: we found the mean contrast in an annulus centered at the inner working angle (90mas) and with a width corresponding to the full-width-at-half-maximum of the point spread function of the telescope. This was done in 10nm increments across 250-500nm passband of the occulter, and the worst of these numbers was taken as a conservative estimate of the worst-case contrast. For the occulter as built, **the worst case contrast was** 2.15×10^{-10}, occurring at 380nm. Figure 8 shows the image-plane intensity at 380nm and Figure 9 shows the resulting mean contrast in the annulus as a function of wavelength in the passband.

It is important to remember the conservatism of this milestone. As can be seen from Figure 9, most wavelengths perform much better than the worst case. In addition, the contrast value is taken right at the

	Perfect structure	As-built structure
Perfect segments	3.1×10^{-12}	1.2×10^{-11}
As-built segments	2.5×10^{-10}	2.1×10^{-10}

Table 2. Worst-case contrast in an annulus about the IWA for four cases: with and without the distortion of the petal structure, and with and without the differences between the ideal edge segments and the shape as built.

smallest inner working angle. Because of the rapid fall-off of the PSF, the contrast quickly improves for only small increases in angle. This again points to the conservatism of our error budget. For instance, one could design a slightly oversized occulter with a smaller inner working angle than required to produce relaxed requirements for the operational inner working angle. As we pointed out earlier, our approach in this TDEM has been to design, build and test the smallest occulter possible for the given mission requirements to verify feasibility.

To find the 95% confidence value we developed a model of the measurement error based on the Allied calibration data for the CMM. Systematic errors in CMM runout were fit and removed, and random errors in the measurement were then modeled based on the residuals. We used this measurement model as the input to a Monte Carlo simulation, where measurement errors consistent with these models were repeatedly applied to the mean of the Allied data. We then evaluated the worst-case mean contrast in an annulus for each of these perturbed data sets. This served to build up a probabilistic model of contrast values consistent with both the petal and the measurement tools; the resulting probability distribution function (PDF) is shown in Fig. 10(a) along with the histogram of Monte-Carlo data. The probability that these results would have occurred had the contrast c actually been greater than 3×10^{-10}—that is, the milestone was not actually met—was numerically indistinguishable from zero. In addition, we find that there is a 95% probability that the true mean-contrast-in-an-annulus is less than 2.16×10^{-10}, bettering our milestone by 30%.

7.2 Performance Estimation for Non-Identical Petals

The results in the previous section assumed each petal on the occulter was identical to the as-built. This is highly conservative and results in an over-estimate of contrast as identical errors rectify around the circumference. A more realistic simulation would populate the occulter with 30 petals containing random errors consistent with the as-built and corresponding error budget. We do this by decomposing the measured data from the segment edges into various error budget terms (for example, amplitude at 2 cycles/meter) and randomizing the amplitude for each segment on each petal around the occulter. This is possible because we can estimate the distribution of manufacturing errors based on the 10 measured optical edge segments. Doing so, however, requires that we assume that each fitted error-budget term on each segment is drawn from the same underlying distribution. In the absence of any other information, this is the only reasonable assumption; with only a single petal manufactured, treating each term on each segment as independent precludes any form of extrapolation. This assumption is not entirely unjustified as each segment is applied along the petal edge using an identical procedure.

After the contrast for the designed petal was determined assuming only global error, some question remained as to why the final contrast estimate was so close to the milestone given the very low contrast (from 1.2×10^{-11} to 6×10^{-11}) computed from the preliminary estimates based on the measured segment shapes. This degradation was due to both errors in the segment placement and counterbend of the segments and from the distortion of the petal structure on which the segments are bonded. Both of these were seen to be present: the measured buttons on the petal structure do not align perfectly between the first (Aug 2011) and second (Feb 2012) measurements at Allied Mechanical, and the measured points along the edges of the petal segments do not align perfectly with the designed petal shape. In particular, a significant uniform bend of the structure was visible in the measured data.

We removed the systematic error in the edge profile due to the distortion of the petal structure by fitting the x- and y- discrepancies in button positions between the first and second Allied runs with a pair of polynomials for each edge, one for each coordinate. We noted that most of the large-scale deformations were

Perturbation	rms Amplitude
Segment δy	15.2 μm
Segment Tilt	25.3 μrad
1 cycle/segment	11 μm
2 cycles/segment	14 μm
3 cycles/segment	5 μm
4 cycles/segment	5 μm
5 cycles/segment	3 μm
6 cycles/segment	3 μm

Table 3. The rms of the fitted amplitude of the most significant perturbation terms on the as-built segments, averaged over the 10 segments. Cyclic terms assume both a sine and cosine wave are present.

from the distortions in the frame. We also noted that the petal-structure deformation is primarily width-preserving, a mode which is known[5] to produce little effect on the contrast when all petals have the same shape. To estimate the relative effect on contrast due to the structure bend, we recomputed the contrast for an occulter with 30 identical petals for four cases: with and without the effects of structure bend, and with and without the effects of segment errors. The results are shown in Table 2. All of these use the February Allied data for the measurements. It appears that some of the structure bend served to compensate for the layout of the segments, though the milestone would have been met even without the distortion present.

In order to fit terms in the error budget we extracted the components normal to the local slope of the petal edge at each point. Table 3 shows the rms averaged amplitudes of the most significant fitted perturbation terms, averaged over all 10 segment fits. A comparison with Table 1 shows that all are below the allocation for a 10^{-10} star shade with the exception of segment tilt that is only slightly above. This implies that an occulter made up of random petals with errors consistent with the measured as-built petal segments (with the structural bend removed) should meet the contrast allocation for manufacturing errors of 1.5×10^{-11} (the structural bend and placement errors are allocated a separate contrast). In fact, a Monte-Carlo analysis using the mean and standard deviations of the perturbations from the 10 as-built segments assuming Gaussian distributions results in a mean contrast due to manufacturing error of 1×10^{-11}.

For further confirmation, we performed a Monte-Carlo analysis that creates new edge segments for the 30 petals by drawing errors from distributions formed based on the 10 measured segments. We used kernel density estimation to create the probability density function for each fitted term.[7,8] Fig. 10(b) shows the resulting distribution of contrasts under the same metric as the manufactured petal (worst-case wavelength, mean of an annulus around the inner working angle) using 50 occulters simulated under the conditions specified above. Two cases were run: one assuming a perfect underlying structure (which should result in a contrast corresponding only to the manufacturing errors described in Section 3) and one with each petal having the identical structural bend to that seen in the as-built petal. We again note the strong assumptions under which these extrapolations were derived, but should those assumptions hold, the modeling suggests that occulter performance will be improved by a factor of more than 10 from the milestone case. Here the expected value of the contrast (assuming a perfect structure) is 2.12×10^{-11} and the 95% confidence value is below 4×10^{-11}. This is slightly larger than the allocation for the flight occulter, but only by a small amount, and gives considerable confidence in our ability to manufacture an occulter to the needed specification.

8. MATERIAL COUPON TESTING

We have also conducted materials tests of representative samples of the M-55J carbon composite used for the TDEM petal. The principal goal of these tests was to assess whether the level of microcracking of the material as the petals are stowed or deployed (or even as they are handled during assembly) is likely to cause a problem with meeting the tight dimensional tolerances required for starlight suppression. Cracking can cause unexpected deformation, and the cracks can act as reservoirs for gases. It may also lead to roughening of the optical edge whose sharpness minimizes undesirable scattering of light. We used mechanical tests,

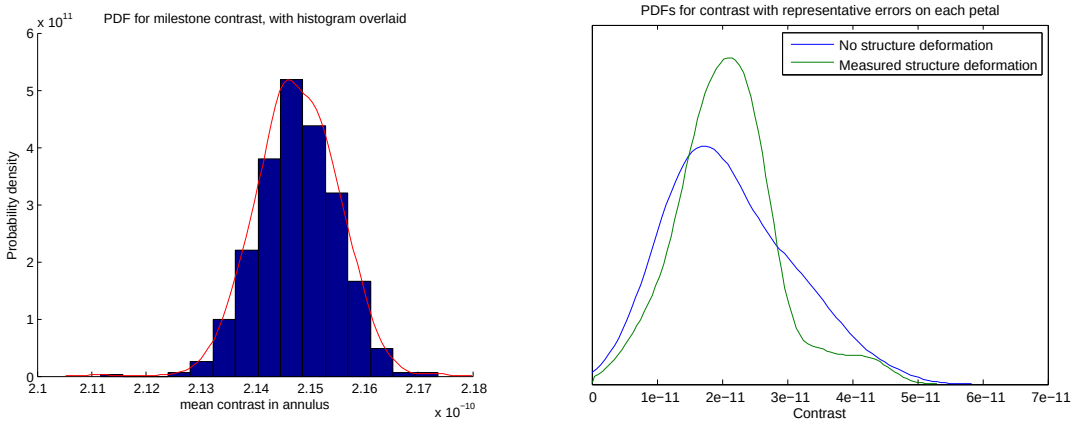

(a) (b)

Figure 10. Probability density functions (PDF) for the true contrast produced by an occulter made from identical copies of the existing petal *(Left)* and random petals with errors consistent with the placed segments applied to each segment on each petal independently *(Right)*. The overlaid histogram in (a) shows the data produced by the Monte-Carlo simulation, representing 700 separate sets of measurement errors. The y-axis normalized the probability density such that the integral over the PDF is 1. In (b), the two cases shown are with and without the overall petal deformation seen in the petal as built.

microscopy, acoustic tomography and small-angle x-ray scattering (SAXS) to characterize the microcracking. These tests found no large cracks (> 100 microns) at bending strains up to 0.5%, the strain at which audible popping occurred. Recall that the petal is designed so that no parts are strained by more than 0.5% during stowing and analysis of the current design shows a maximum strain of only 0.2%. The stress-strain curves did not display any anomalies until a precipitous drop in stress at a strain of $\sim 1.2\%$ due to the formation of a transverse crack. Analysis of SAXS data is on-going which will quantify microcrack distributions at the sub-micron level. We also note that the targeted material for flight, M-46J, has a much higher strain capability.

9. FINAL REMARKS

Over the course of the two year TDEM project we demonstrated our ability to manufacture a petal to flight-like processes and measure the shape with enough precision to meet our milestone requirement. In fact, we exceeded our milestone goal by 30% in contrast at the worst case wavelength and closest inner working angle for the conservative case of a single set of global errors on all petals equal to that on our measured as-built petal. For the more realistic case of an occulter with random errors on each petal consistent with those seen on the as-built petal we achieved a calculated mean contrast at the inner working angle more than an order of magnitude better than the milestone (more than a factor of 5 better at the 95% confidence level). We have thus shown that it is possible to build an occulter petal to the stringent shape requirements for a terrestrial planet finding mission.[‡]

Note that we do not claim to have developed an optimal design and manufacturing process for the occulter petal. For instance, more exploration of cutting techniques and metrology methods is certainly warranted. We also discovered the need for additional support to eliminate the structural bend. Our goal, however, was only to demonstrate that a design exists, that it can be built to the stringent requirements needed for an

[‡]Experiments are being undertaken in the laboratory at Princeton to verify the validity of the numerical optical modeling used to compute the contrast from the shape. Current results show that a scaled occulter mask, designed using the same modeling and optimization approaches as the large space version, is achieving contrast consistent with predictions.[9] This provides confidence that at the level of contrast in this TDEM the modeling used to confirm the milestone is accurate.

occulter mission, and that existing metrology techniques are sufficient to demonstrate performance. In that we succeeded. More importantly, we learned a great deal about the design and manufacture of petals that can be applied to future work on starshade missions. We have kept careful track of the "lessons learned" and expect to apply them in our next iteration of petal manufacture.

Acknowledgements

This work was partially performed under a grant from the National Aeronautics and Space Administration (NASA), grant number NNX10AF83G. This work was partially carried out at the Jet Propulsion Laboratory, California Institute of Technology, under contract to NASA. The work of Macintosh, Rudd and Savransky was performed under the auspices of the U.S. Department of Energy by Lawrence Livermore National Laboratory under Contract DE-AC52-07NA27344.

REFERENCES

1. R. Vanderbei, E. Cady, and N. Kasdin, "Optimal occulter design for finding extrasolar planets," *Astrophysical Journal* **665**, pp. 794–798, 2007.
2. D. Savransky, D. N. Spergel, N. J. Kasdin, E. J. Cady, P. D. Lisman, S. H. Pravdo, S. B. Shaklan, and Y. Fujii, "Occulting ozone observatory science overview," in *Proceedings of the SPIE Astronomical Instrumentation Conference*, *7731*(88), 2010.
3. M. W. Thomson, P. D. Lisman, R. Helms, P. Walkemeyer, A. Kissil, O. Polanco, and S. Lee, "Starshade design for occulter based exoplanet missions," in *Proceedings of the SPIE Astronomical Instrumentation Conference*, *7731*(191), 2010.
4. S. B. Shaklan, L. F. Marchen, D. Lisman, E. J. Cady, S. R. Martin, N. J. Kasdin, and P. J. Dumont, "A starshade petal error budget for exo-earth detection and characterization," in *Proceedings of the SPIE Conference on Optics and Photonics*, *8151*(38), 2011.
5. S. B. Shaklan, M. C. Noecker, T. Glassman, A. S. Lo, P. J. Dumont, N. J. Kasdin, E. J. Cady, R. Vanderbei, and P. R. Lawson, "Error budgeting and tolerancing of starshades for exoplanet detection," *Space Telescopes and Instrumentation 2010: Optical, Infrared, and Millimeter Wave* **7731**(1), p. 77312G, SPIE, 2010.
6. E. Cady, "Boundary diffraction wave integrals for diffraction modeling of external occulters," *Optics Express* **20**, pp. 15196–15208, July 2012.
7. B. A. Turlach, *Bandwidth selection in kernel density estimation: a review*, CORE and Institut de Statistique, 1993.
8. B. W. Silverman, *Density estimation for statistics and data analysis*, 1986.
9. D. Sirbu, N. J. Kasdin, and R. J. Vanderbei, "Further optical verification of occulter-based high contrast imagine," in *Proceedings of the SPIE Astronomical Instrumentation Conference*, *8442*(18), 2012.